

Photoelectron spectroscopy and theoretical studies of PCSe^- , AsCS^- , AsCSe^- , and NCSe^- : Insights into the electronic structures of the whole family of ECX^- ($E = \text{N, P, and As}$; $X = \text{O, S, and Se}$) anions

Qinqin Yuan,^[a] Frank Tambornino,^{[b][c]} Alexander Hinz,^[d] Weston Thatcher Borden,^[e] Jose M.

Goicoechea,^{*[b]} Bo Chen,^{*[f]} Xue-Bin Wang ^{*[a]}

Abstract: The newly synthesized, phosphorus- and arsenic-containing analogues, PCSe^- , AsCS^- , and AsCSe^- , of the thio- and seleno-cyanate anions, as well as the known ion NCSe^- , were investigated in the gas phase by negative ion photoelectron spectroscopy (NIPES), velocity-map imaging (VMI) spectroscopy, and quantum chemical computations. The electron affinities (EA), spin-orbit (SO) splittings, and “symmetric” / “antisymmetric” stretching frequencies (ν_1 and ν_3) of the neutral radicals, ECX^\bullet ($E = \text{N, P and As}$, $X = \text{S and Se}$), generated by electron detachment from the corresponding anions, were obtained from the spectra. The calculated EAs, SO splittings, and vibrational frequencies are in excellent agreement with the measured values. These newly obtained values, when combined with those previously determined for the lighter analogues, show interesting trends on descending the pnictogen and chalcogen series. These trends are rationalized on the basis of electronegativity arguments, the electron distribution in the HOMO, and NBO/NRT analyses.

The chemistry of the archetypal pseudohalide ions, cyanate (NCO^-) and thiocyanate (NCS^-), particularly their role as ambidentate nucleophiles, has been extensively studied and is described in many textbooks on fundamental inorganic chemistry.^[1] Heavier analogues of ECX^- ($E = \text{pnictogen}$; $X = \text{chalcogen}$), such as the 2-phosphaethynolate (PCO^-) and 2-phosphathioethynolate (PCS^-) anions, were first reported by

Becker and co-workers as lithium salts in 1990s. However, their reactivity remained largely unexplored for two decades.^[2]

New synthetic routes allowing for the bulk preparation and isolation of PCO^- were reported in 2011 and 2013,^[3,4] paving the way for the exploration of its chemical reactivity. It has been demonstrated that PCO^- is a viable precursor for the synthesis of novel phosphorus-containing compounds.^[4–11] More recently, synthetic methods allowing for the isolation of bulk quantities of heavier ECX^- ($E = \text{P, As}$; $X = \text{O, S, Se}$) species have become available, enabling comparative studies of the bonding and reactivity profiles of this interesting library of anions. For example, AsCO^- was isolated by Goicoechea in 2016,^[12] and found to play important role in the formation of arsenic-containing compounds.^[12–14] The long-sought, PCSe^- , AsCS^- , and AsCSe^- ions were also synthesized and characterized by Goicoechea's group in 2018.^[10]

Triatomic pseudohalide anions ECX^- are extensively employed in coordination chemistry and organic synthesis.^[15–18] Electron delocalization over the three atoms gives rise to three predominant resonance structures ($\text{E}\equiv\text{C}-\text{X}^-$, $^-\text{E}=\text{C}=\text{X}$, and $2^-\text{E}-\text{C}\equiv\text{X}^*$).^[4, 12, 19] Previous studies have shown that the relative weights of these resonances vary with the nature of E and X ,^[4, 10, 12, 13, 19] and that, consequently, the ions differ in their behavior and in their reactivity towards Lewis acids. For example, the cyanate (NCO^-) and thiocyanate anions (NCS^-) are dominated by the $\text{E}\equiv\text{C}-\text{X}^-$ resonance structure. However, in the case of their phosphorus-containing analogues, PCO^- and PCS^- , the $^-\text{E}=\text{C}=\text{X}$ resonance structure has an increased weight according to natural resonance theory (NRT) analysis.^[13]

The change in the relative contributions of resonance structures of these anions gives rise to different coordination modes towards electrophiles. For instance, it has been shown that NCO^- binds many metals (Th, U, Re and W)^[15, 16] through the nitrogen atom, whereas PCO^- coordinates with either the phosphorus or oxygen atoms, depending on the metal (P to W or Re^[16, 20], and O to Th or U^[15]). However, for PCS^- , both P- and S-coordination to the same metal (W) were observed.^[16]

Negative ion photoelectron spectroscopy (NIPES) and high-level quantum chemical calculations were carried out, in order to investigate the intrinsic molecular properties of the anions – NCO^- , NCS^- , PCO^- , PCS^- , AsCO^- – and of the corresponding neutral radicals – NCO^\bullet , NCS^\bullet , PCO^\bullet , PCS^\bullet and AsCO^\bullet – formed via photodetachment of the anions.^[13, 21] Compared to NCO^- , NCS^- , PCO^- and PCS^- , the heavier arsenic-containing ion (AsCO^-) possesses a smaller electron binding energy, a different weighting of resonance structures, and a larger spin-orbit (SO) splitting. The electronic structure information, bonding

- [a] Ms. Q. Yuan, Dr. X.-B. Wang
Physical Sciences Division, Pacific Northwest National Laboratory
902 Battelle Boulevard, P. O. Box 999, MS K8-88, Richland,
Washington 99352, USA
E-mail: xuebin.wang@pnnl.gov
- [b] Dr. F. Tambornino, Prof. Dr. J. M. Goicoechea
Department of Chemistry, University of Oxford, Chemistry Research
Laboratory, 12 Mansfield Road, Oxford, OX1 3TA, UK
E-mail: jose.goicoechea@chem.ox.ac.uk
- [c] Dr. F. Tambornino
Fachbereich Chemie, Philipps-Universität Marburg, Hans-Meerwein-
Strasse 4, 35043 Marburg, Germany
- [d] Dr. A. Hinz
Karlsruhe Institut of Technology (KIT), Institute for Inorganic
Chemistry (AOC), Engesserstraße 15, Geb. 30.45, 76131 Karlsruhe,
Germany
- [e] Prof. Dr. W.T. Borden
Department of Chemistry and the Center for Advanced, Scientific
Computing and Modeling, University of North Texas, 1155 Union
Circle, #305070, Denton, Texas 76203-5070, USA
- [f] Dr. B. Chen
Department of Chemistry, Pennsylvania State University, University
Park, Pennsylvania, 16801, USA
E-mail: cberic@hotmail.com

analyses, and quantitative characterization of resonance structures for these species provide a molecular-level basis to rationalize their diverse chemistry.

The newly synthesized, phosphorus- and arsenic-containing analogues of the thio- and seleno-cyanate anions, ECX^- ($E = P, As$; $X = S, Se$) are expected to exhibit a different reactivity profile and relatively poor nucleophilicity, compared to their lighter homologues. This is because the negative charge shifts from the terminal pnictogen and chalcogen atoms to the central carbon atom of the anion, due to the decrease of the electronegativity of the terminal atoms.^[10] In order to quantitatively determine these particular properties, and to lay a molecular foundation for understanding the chemistry and coordination behavior of these species, we have used NIPES and ab initio computations, to probe the electronic structures and chemical properties of $PCSe^-$, $AsCS^-$, $AsCSe^-$, and $NCSe^-$ in the gas phase. The information thus obtained completes the 3×3 molecular property matrix across the whole family of ECX^- ($E = N, P, As$; $X = O, S, Se$) anions and the ECX^\bullet radicals formed from them.

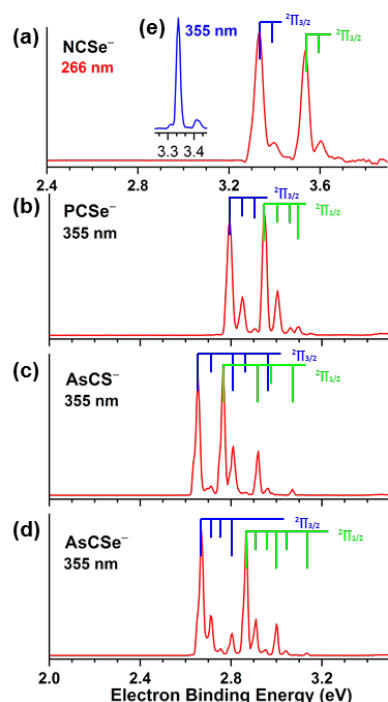


Figure 1. 20 K NIPES spectra of (a) $NCSe^-$ at 266 nm, (b) $PCSe^-$, (c) $AsCS^-$ and (d) $AsCSe^-$ at 355 nm. Two vibrational progressions (indicated with long (ν_3) and short (ν_1) vertical lines) in each of the spin-orbit electronic states, $^2\Pi_{3/2}$ (blue) and $^2\Pi_{1/2}$ (green), are labeled. The 355 nm spectrum of (e) $NCSe^-$, inserted in panel (a), shows a better resolved vibrational progression than the 266 nm spectrum of $NCSe^-$.

Figure 1 shows the 20 K NIPES spectra of $NCSe^-$ at 266 nm (4.661 eV), and $PCSe^-$, $AsCS^-$, $AsCSe^-$, obtained at 355 nm (3.496 eV). The 266 nm spectrum of $NCSe^-$ shows two dominant peaks in the range of 3.2 to 3.7 eV; while the three 355 nm spectra exhibit well-resolved multiple peaks between 2.6 and 3.2 eV. The adiabatic detachment energy (ADE) of each anion, or, equivalently, the electron affinity (EA) of each neutral radical, was determined from the 0–0 transition. The EAs were found to increase in the order of $AsCS^-$ (2.655 eV) < $AsCSe^-$ (2.670 eV) < $PCSe^-$ (2.795 eV) < $NCSe^-$ (3.330 eV). In addition, we also obtained the 20 K photoelectron imaging

spectra of $AsCS^-$ and $AsCSe^-$, measured with 440 nm photons (Figure S1).

Combined with the previous NIPES results for ECX^\bullet ,^[13, 21] the EAs are found to decrease on descending group 15, for $E = N, P$, and As . For example, NCO^\bullet (3.609 eV)^[21] > PCO^\bullet (2.670 eV)^[13] > $AsCO^\bullet$ (2.414 eV);^[13] NCS^\bullet (3.537 eV)^[21] > PCS^\bullet (2.850 eV)^[13] > $AsCS^\bullet$ (2.655 eV); and $NCSe^\bullet$ (3.330 eV) > $PCSe^\bullet$ (2.795 eV) > $AsCSe^\bullet$ (2.670 eV).

However, on varying the group 16 elements, X , the EAs present different trends between the three series, depending on the identity of E . For example, for $E = N$, the EAs again decrease on descending the periodic table from $X = O$ to $X = S$, to $X = Se$. Thus, NCO^\bullet (3.609 eV) > NCS^\bullet (3.537 eV) > $NCSe^\bullet$ (3.340 eV). In contrast, for $E = As$ the EAs increase on moving down group 16, so that $AsCO^\bullet$ (2.414 eV) < $AsCS^\bullet$ (2.655 eV) < $AsCSe^\bullet$ (2.670 eV). For $E = P$ the changes in the EAs on descending group 16 are not monotonic, with PCO^\bullet (2.670 eV) < PCS^\bullet (2.850 eV) > $PCSe^\bullet$ (2.795 eV). The origins of these unusual phenomena will be discussed below.

Similar to the previous spectra of NCO^- , NCS^- , PCO^- , PCS^- , and $AsCO^-$,^[13, 21] each of the four spectra in this work also consists of two sets of peaks that are similar in appearance. The spacing between the corresponding peaks of the two sets are attributed to the spin-orbit (SO) splitting of the spin-free $^2\Pi$ states of the $NCSe^\bullet$, $PCSe^\bullet$, $AsCS^\bullet$, and $AsCSe^\bullet$ radicals into $\Omega = 3/2$ and $1/2$ components. The values of SO splitting for these four triatomic species were determined from the spacing between the two strongest peaks in the NIPES spectrum as 1653 cm^{-1} , 1250 cm^{-1} , 887 cm^{-1} , 1573 cm^{-1} for $NCSe^\bullet$, $PCSe^\bullet$, $AsCS^\bullet$, and $AsCSe^\bullet$, respectively (Figure 1 and Table 1). The SO splittings, measured from other doublets in the NIPES spectra, are nearly identical to the SO splittings, measured from the 0–0 peaks.

Table 1. Comparison of the measured and calculated electron affinities (EAs), spin-orbit (SO) splittings, and unscaled harmonic vibrational frequencies of the two stretching modes in $NCSe^\bullet$, $PCSe^\bullet$, $AsCS^\bullet$, and $AsCSe^\bullet$. The EAs in parentheses contain zero-point vibrational energy corrections.

ECX^\bullet	EA (eV)		SO splitting (cm^{-1})		Frequency (cm^{-1})	
	Expt. ^a	Calc.	Expt. ^a	Calc. ^e	Expt. ^a	Calc. ^f
$NCSe^\bullet$	3.330	3.38 (3.38) ^b 3.34 ^c 3.40 (3.39) ^d	1653	1670	565, N/A	563, 2118 ^b 560, 2097 ^d
$PCSe^\bullet$	2.795	2.89 (2.88) ^b 2.82 ^c 2.81 (2.80) ^d	1250	1232	470, 1210	474, 1223 ^b 480, 1238 ^d
$AsCS^\bullet$	2.655	2.76 (2.76) ^b 2.70 ^c 2.63 (2.63) ^d	887	914	457, 1250	491, 1273 ^b 479, 1276 ^d
$AsCSe^\bullet$	2.670	2.75 (2.74) ^b 2.70 ^c 2.70 (2.69) ^d	1573	1573	350, 1089	358, 1103 ^b 360, 1127 ^d

^a Experimental uncertainty is 0.005 eV for EA, and 20 cm^{-1} for SO splitting and frequency. ^b Calculated at the (U)CCSD(T)/aug-cc-pVTZ level. ^c Calculated at the (8/6) and (7/6) CASPT2/aug-cc-pVTZ(-PP) level. ^d Calculated at the (U)B3LYP/aug-cc-pVTZ level. ^e MR-CISD with (15/12)CASSCF/cc-pVTZ-DK reference wavefunction. ^f The error bar of the computed frequencies is estimated to be 30 cm^{-1} .

In addition, each series of peaks ($^2\Pi_{3/2}$ or $^2\Pi_{1/2}$) consists of two sets of vibrational progressions that can be assigned to the

“symmetric” stretching mode (ν_1), with a lower frequency, and the “antisymmetric” stretching mode (ν_3), with a higher frequency for each ECX^\bullet radical. It is straightforward to obtain the two vibrational frequencies from each set of peaks of the NIPE spectrum of $AsCS^-$ (ν_1 : 457 and ν_3 : 1250 cm^{-1}) and $AsCSe^-$ (ν_1 : 350 and ν_3 : 1089 cm^{-1}). However, the antisymmetric stretching mode (ν_3 : 1210 cm^{-1}) for $PCSe^\bullet$ can only be measured for the $^2\Pi_{1/2}$ state, because the ν_3 fundamental excitation peak in the $^2\Pi_{3/2}$ series overlaps with the origin of the $^2\Pi_{1/2}$ state. The “symmetric” stretching mode for $PCSe^\bullet$ is measured to be $\nu_1 \approx 470$ cm^{-1} and to be $\nu_1 \approx 565$ cm^{-1} for $NCSe^\bullet$. The “antisymmetric” stretching frequency of $NCSe^\bullet$ could not be obtained, due to the absence of this vibration from the spectrum.

All of the experimental EAs, SO splittings, and the vibrational frequencies of the two stretching modes in $NCSe^\bullet$, $PCSe^\bullet$, $AsCS^\bullet$, and $AsCSe^\bullet$ are shown in Table 1, where comparisons are made with computed values, obtained using the B3LYP, CASPT2, and/or CCSD(T) methods. Additional CCSD(T) computations of EAs using the improved aug-cc-pV(T+d)Z basis set,^[22] which is purportedly better for calculating species containing S and P atoms, yielded better agreement with experiment (see Table S1). In general, excellent agreement is evident among different computational methods and between the experiments and the calculations.

The computed (U)CCSD(T) bond lengths of ECX^\bullet/ECX^\bullet are shown in Table 2. (See Table S2 in the SI for bond distances computed with other methods and basis sets). Comparison with the experimental bond distances in the anions shows that the CCSD(T) calculations overestimate the lengths of most of the bonds in the anions, but by less than 0.1 Å. Previous calculations at the $\omega B97XD/Def2-QZVP$ level with a PCM solvation model achieved a better agreement with experiment.^[10] Note that these anions distort slightly from a linear geometry in the solid state but are linear in the optimized gas phase structures. Cyclic isomers of these anions were also calculated and found to be over 40 kcal/mol higher in energy than the linear isomers (See Table S3).

Table 2. Experimental and (U)CCSD(T)/aug-cc-pVTZ bond distances in ECX^\bullet and ECX^\bullet .

	$E-C$ distance (Å)		$C-X$ distance (Å)	
	Expt. ^a	CCSD(T)	Expt. ^a	CCSD(T)
$NCSe^-$	1.162(4)	1.179	1.801(3)	1.825
$NCSe^\bullet$		1.173		1.802
$PCSe^-$	1.46(3)/1.53(7)	1.602	1.78(3)/1.85(7)	1.788
$PCSe^\bullet$		1.596		1.751
$AsCS^-$	1.691(5)	1.721	1.605(5)	1.634
$AsCS^\bullet$		1.739		1.578
$AsCSe^-$	1.699(4)	1.714	1.745(4)	1.781
$AsCSe^\bullet$		1.725		1.733

^a from ref 10.

In order to analyze the trends in the EAs and SO splittings in the nine ECX^\bullet radicals ($E = N, P, As$ and $X = O, S, Se$), we show the EAs and SO splittings in a 3×3 matrix in Figure 2. Also shown in Figure 2 are the shapes of HOMOs of the ECX^\bullet anions, which, as would be expected, are very similar to the shapes of the SOMOs of the ECX^\bullet radicals (Figure S2).

As noted above, the EAs decrease on descending all three of the columns in Figure 2, a phenomenon that can be readily understood on the basis of the electronegativities of the pnictogens, E ($N > P > As$) in ECX^\bullet . However, such a simple electronegativity argument cannot explain the completely different EA trends across the three rows, where the EA decreases in the NCX^\bullet series ($X = O \rightarrow S \rightarrow Se$), increases and then decreases in the PCX^\bullet series, and increases in the $AsCX^\bullet$ series.

The electron distribution in the HOMOs provides an explanation of these puzzling results. Similar to the valence isoelectronic CO_2 molecule, each ECX^\bullet anion has two degenerate HOMOs, only one of which is shown in Figure 2. But unlike CO_2 , where the molecular symmetry ($D_{\infty h}$) guarantees zero coefficient of the HOMOs on the C atom and equal coefficients on the two O atoms, the lowered symmetry in ECX^\bullet anions ($C_{\infty v}$) results in nonzero coefficients on C and unequal coefficients on E and X.

Careful inspection of Figure 2 shows that in the HOMOs of ECX^\bullet , the C has a bonding π interaction with the pnictogen, E, albeit a weak one in NCS^- and $NCSe^-$. Figure 2 also shows that the less electronegative the chalcogen atom, the greater its coefficient in the HOMO.

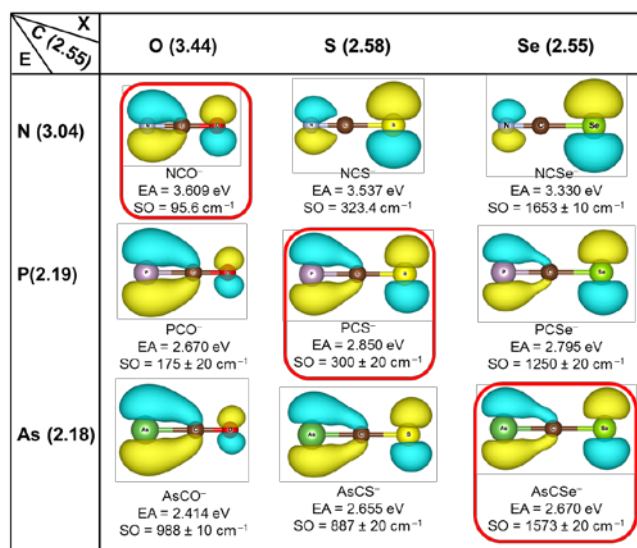


Figure 2. The experimental EAs and SO splittings of nine ECX^\bullet radicals, the calculated HOMOs of the ECX^\bullet anions, and the Pauling electronegativities of the constituent atoms (in parentheses). The anions in the same column differ by only the pnictogen atom E, and in the same row by only the chalcogen atom X. The species circled in red have the highest EA in their respective rows. The HOMOs were calculated at B3LYP/aug-cc-pVTZ level of theory and plotted with isovalue = 0.07. As would be expected, the HOMOs of the ECX^\bullet anions are similar in appearance to the SOMOs of ECX^\bullet radicals, which are shown in Figure S2.

The relative EAs of ECX^\bullet can be explained by qualitatively assessing the relative ease of removing one electron from each of the ECX^\bullet HOMOs in Figure 2. The relative ease or difficulty of removing one electron from each of the HOMOs is, of course, affected by the electronegativities of E and X. However, the EAs are affected not just by the relative electronegativities of E and X but also by the electron distribution in each HOMO. Therefore, the crucial factor in determining the relative EAs of

ECX^{\bullet} is the electronegativity of the atom that makes the largest contribution to the HOMO.

For example, descending either of the three columns in Figure 2, there is clear increase in the coefficient on the pnictogen, E , and a decrease in the coefficient on the chalcogen X . As the pnictogen becomes less electronegative than the chalcogen, the shift in the electron density to the pnictogen atom results in the observed EA reduction down each of the $X = O, S$, and Se columns in Figure 2.

Moving across the rows of Figure 2, the coefficient of the chalcogen, X , in the HOMO can be seen to increase at the expense of the coefficient of the pnictogen, E , as the chalcogen becomes less electronegative ($X = O \rightarrow S \rightarrow Se$). For $E = N$, the chalcogens $X = S$ and Se are less electronegative than the pnictogen; so the EA decreases across the first row of Figure 2.

In contrast, in the third row of Figure 2, the pnictogen, $E = As$ is less electronegative than all three of the chalcogens, $X = O, S$, and Se . Consequently, as the coefficient of the chalcogen in the HOMO increases on going from $O \rightarrow S \rightarrow Se$, the EA increases.

In the second row of Figure 2, the increase in the coefficient on the chalcogen for $X = O \rightarrow S$ results in an increase in the EA, since S is more electronegative than the pnictogen, $E = P$. However, as shown in Figure 2, $X = S \rightarrow Se$ results in very little change in the relative sizes of the coefficients on the pnictogen and on the chalcogen atoms. Therefore, in this case the lower electronegativity of Se , relative to S , apparently is dominant; and this makes the EA of $PCSe^{\bullet}$ slightly lower than that of PCS^{\bullet} .

Based on this type of analysis of the effects of electronegativity changes on the HOMOs of ECX^{\bullet} , we previously predicted that the then unknown $AsCS^{\bullet}$ radical should have a higher EA than that of $AsCO^{\bullet}$ radical.^[13] Without understanding the effect that the substitution $X = O \rightarrow S$ has on the shape of the HOMOs, the prediction that the substitution of the less electronegative atom, S , for the more electronegative atom, O , should raise the EA would be counterintuitive. However, this prediction is confirmed by the experimental EAs, obtained in this study for $AsCS^{\bullet}$ and $AsCO^{\bullet}$ in Table 1.

Our NBO computations show the same trends in the composition of the HOMOs depicted in Figure 2 (see Table S4 in the SI). In general, there are three major contributors to the HOMO: a π bonding natural orbital between E and C , the corresponding π^* orbital and a lone-pair orbital on X . Among these three contributors, the π^* contribution is the smallest.

For the ECO^- anions, the π bonding orbital contribution is dominant, but for ECS^- and $ECSe^-$, the lone-pair orbital is the largest contributor. Within any of the three series of ECO^- , ECS^- and $ECSe^-$ anions ($E = N, P, As$), the π bonding orbital contributions increase the heavier the pnictogen is; and, correspondingly, the lone-pair orbital becomes less important. These trends are not reflected directly in the observed EAs, but the differences in the π bonding and lone-pair orbital contributions correlate nicely with the observed EAs.

It is found that, within the series of NCX^{\bullet} , PCX^{\bullet} and $AsCX^{\bullet}$ ions, the smaller the difference in the two dominant orbital contributions, the higher the EA is in general. This can be interpreted as meaning that the more similar the shape and energy of the atomic orbitals of the terminal atoms are, the more these AOs will both contribute to the HOMO. Consequently, the more delocalised over the whole ion the additional electron added to the ECX^{\bullet} radical is, the higher the EA will be. Note that a larger extent of delocalisation leads to a smaller dipole moment of the radical. Therefore, as shown in

Table S5, the smaller the dipole moment of the radical, the higher the EA is in general.

This trend can clearly be seen in Figure 2, where the HOMOs of the molecules circled in red are the most delocalized; and these ECX^{\bullet} radicals each have the highest EA value in their row. This trend is also reflected in the NRT computations, where the EA values among $AsCO^{\bullet} < AsCS^{\bullet} < AsCSe^{\bullet}$, $PCO^{\bullet} < PCS^{\bullet} \sim PCSe^{\bullet}$ are correlated with the contribution of the $E \equiv C-X^{\bullet}$ resonance structure (see Table S6).

The calculated SO splittings for each ECX^{\bullet} species match very well with the experimental values, i.e., 1670 vs. 1653 cm^{-1} for $NCSe^{\bullet}$; 1232 vs. 1250 cm^{-1} for $PCSe^{\bullet}$; 914 vs. 887 cm^{-1} for $AsCS^{\bullet}$; and 1573 vs. 1573 cm^{-1} for $AsCSe^{\bullet}$. Obviously, the ECX^{\bullet} radicals, containing the heavier main group elements (As and Se) have significantly larger SO splittings, approaching 1000 cm^{-1} , than their lighter congeners containing only the elements N, P, O and S . The SO splittings of the latter are determined to be less than or ~ 300 cm^{-1} .^[13,21] The SO splittings of 1573 cm^{-1} for $AsCSe^{\bullet}$ and 1653 cm^{-1} for $NCSe^{\bullet}$ are the largest observed among all of the ECX^{\bullet} radicals to date.

It is worth noting that the SO splitting in $AsCO^{\bullet}$ (988 cm^{-1})^[13] is slightly larger than that in $AsCS^{\bullet}$ (887 cm^{-1}), and the SO splitting of $NCSe^{\bullet}$ (1653 cm^{-1}) is larger than that of $PCSe^{\bullet}$ (1250 cm^{-1}). These findings contrast with the naive expectation that spin-orbit coupling (SOC) should increase as Z^2 for multi-electron atoms,^[23] where Z is the effective nuclear charge.

However, in addition to atomic number, the electron distribution in the SOMO also determines the SO splitting in ECX^{\bullet} . The larger the coefficient (i.e., the larger electron density) on the heavier atoms, the bigger the SO splitting. For example, in the case of $AsCO^{\bullet}$ vs $AsCS^{\bullet}$, Figure 2 indicates that the SOMO has a larger coefficient on the As atom in $AsCO^{\bullet}$ than in $AsCS^{\bullet}$ (due to the larger electronegativity difference between As and O than between As and S).

Moving to the next member of the $AsCX^{\bullet}$ series, $AsCSe^{\bullet}$, the small electronegativity change from S to Se leads to a small electron distribution change in the SOMOs of $AsCS^{\bullet}$ and $AsCSe^{\bullet}$. Therefore, one would not expect a big change in SO splitting from $AsCS^{\bullet}$ to $AsCSe^{\bullet}$, based solely on electron distribution in the SOMOs. However, the actual increase of the SO splitting from 887 cm^{-1} in $AsCS^{\bullet}$ to 1573 cm^{-1} in $AsCSe^{\bullet}$ is very large, and this increase is almost certainly associated with the presence of a second, very heavy atom, Se , in $AsCSe^{\bullet}$.

In $NCSe^{\bullet}$, Figure 2 indicates that almost all electron density in the SOMO is concentrated on the heavy Se atom. This leads to $NCSe^{\bullet}$ having the largest SO splitting (1653 cm^{-1}) among all nine of the ECX^{\bullet} radicals.

Figure 3 and Table S7 show the calculated Franck-Condon factors (FCFs) for the vibrational peaks in the transitions from anion to radical for four ECX^- anions. The simulated stick spectra of ECX^{\bullet} include two sets of vibrational progressions, although only the "symmetric" stretching mode is excited in the $NCSe^{\bullet}$ case.

Since both the ECX^- anions and the ECX^{\bullet} radicals have linear gas-phase geometries, the two sets of vibrational progressions observed must arise from the two stretching modes ("symmetric" ν_1 and "antisymmetric" ν_3) that retain the linear geometry of the molecule. The bending modes (Table S8) that destroy the linear geometry do not produce vibrational peaks in the NIPE spectra.

In order to take into account the SO splitting observed in the experimental spectra, each FC stick in the simulated stick spectra was split into a doublet with equal intensity (blue sticks

and green sticks), separated by the experimentally observed SO splitting. Finally, the simulated spectra (grey lines) were produced by replacing each stick with a Gaussian of 20 meV full-width at half-maximum (fwhm) for the 355 nm spectra, and 30 meV fwhm for the 266 nm spectrum. Figure 3 shows that the simulated NIPE spectra agree very well with the experimental NIPE spectra.

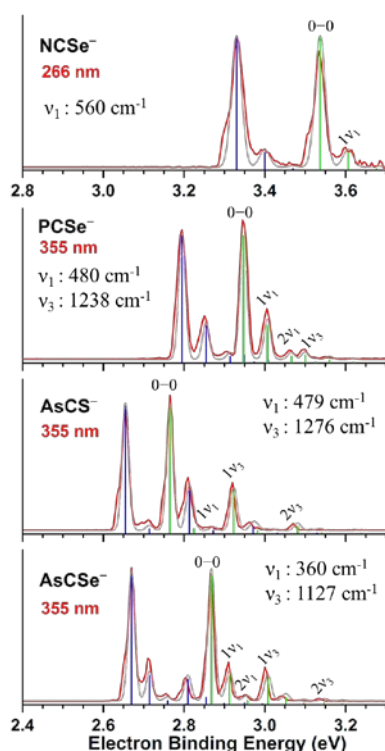


Figure 3. The vibrational peaks in the B3LYP/aug-cc-pVTZ simulated NIPE stick spectra of NCSel^- , PCSe^- , AsCS^- , and AsCSe^- , separated by the corresponding spin-orbit splitting ($^2\Pi_{3/2}$ blue; $^2\Pi_{1/2}$ green). The 0-0 peak and vibrational progressions, due to the symmetric and antisymmetric stretching modes (ν_1 and ν_3), are indicated in the $^2\Pi_{1/2}$ stick spectra. Convolved spectra were produced by replacing each stick with a Gaussian of 20 meV full-width at half-maximum (fwhm) for the 355 nm spectra, and 30 meV fwhm for the 266 nm spectrum. The convolved spectra (grey) are superimposed onto the experimental 355 nm NIPE spectrum (red) for PCSe^- , AsCS^- , and AsCSe^- , and the 266 nm NIPE spectrum (red) for NCSel^- . CCSD(T) simulations gave very similar results and are included in the Figure S3 and S4.

In conclusion, we have conducted NIPES experiments and performed quantum chemical computations on NCSel^- and on PCSe^- , AsCS^- , and AsCSe^- , the three newest members of the ECX^- family (E = pnictogen, X = chalcogen). The geometries, electronic structures, SO splittings, and vibrational frequencies of these anions and their radical neutrals were computed and used to simulate the experimental NIPE spectra. The calculated EAs, SO splittings, and vibrational frequencies agree very well with experimentally-measured values.

These newly determined EAs and SO splittings, serve as critical data to complete the 3×3 matrixes of EA and SO values for the ECX^- family, from the 1st to the 3rd row of both pnictogen and chalcogen atoms. We find that the observed trends in EA

and SO values cannot be understood on the basis of just the electronegativities and atomic numbers of the atoms in the ECX^- anions and ECX^\bullet radicals. Instead, how the identities of the atoms affect the electron distributions in the HOMOs of the ECX^- anions and in the SOMOs of the radicals play a critical role in determining both the EA and SO values.

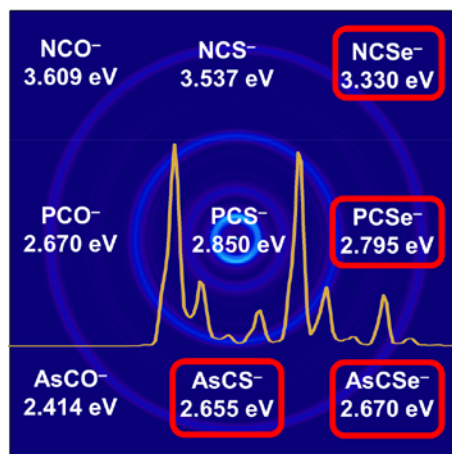
Acknowledgements The NIPES work done at the Pacific Northwest National Laboratory was supported by the U.S. Department of Energy, Office of Science, Office of Basic Energy Sciences, Division of Chemical Sciences, Geosciences and Biosciences. Most of the computations were done on the CASCAM cluster at University of North Texas. F. Tambornino gratefully acknowledges the DFG for funding (No. FT 1357/1-1).

Keywords: electron affinity • SO Splitting • HOMOs • photoelectron spectroscopy

References

- [1] A. Earnshaw, N. N. Greenwood, *Chemistry of the Elements*, Vol. 60, Butterworth-Heinemann Oxford, **1997**.
- [2] G. Becker, W. Schwarz, N. Seidler, M. Westerhausen, *Z. Anorg. Allg. Chem.* **1992**, 612, 72-82.
- [3] F. F. Puschmann, D. Stein, D. Heift, C. Hendriksen, Z. A. Gal, H. F. Grützmacher, H. Grützmacher, *Angew. Chem. Int. Ed.* **2011**, 50, 8420-8423.
- [4] A. R. Jupp, J. M. Goicoechea, *Angew. Chem. Int. Ed.* **2013**, 52, 10064-10067.
- [5] D. Heift, Z. Benkő, H. Grützmacher, A. R. Jupp, J. M. Goicoechea, *Chem. Sci.* **2015**, 6, 4017-4024.
- [6] L. Liu, D. A. Ruiz, D. Munz, G. Bertrand, *Chem* **2016**, 1, 147-153.
- [7] Y. Xiong, S. Yao, T. Szilvási, E. Ballester-Martínez, H. Grützmacher, M. Driess, *Angew. Chem.* **2017**, 129, 4397-4400.
- [8] A. R. Jupp, J. M. Goicoechea, *J. Am. Chem. Soc.* **2013**, 135, 19131-19134.
- [9] A. Hinz, R. Labbow, C. Rennick, A. Schulz, J. M. Goicoechea, *Angew. Chem. Int. Ed.* **2017**, 56, 3911-3915.
- [10] F. Tambornino, A. Hinz, R. Köppe, J. M. Goicoechea, *Angew. Chem. Int. Ed.* **2018**, 57, 8230-8234.
- [11] L. Weber, *Eur. J. Inorg. Chem.* **2018**, 2018, 2175-2227.
- [12] A. Hinz, J. M. Goicoechea, *Angew. Chem.* **2016**, 128, 8678-8683.
- [13] G.-L. Hou, B. Chen, W. J. Transue, Z. Yang, H. r. Grützmacher, M. Driess, C. C. Cummins, W. T. Borden, X.-B. Wang, *J. Am. Chem. Soc.* **2017**, 139, 8922-8930.
- [14] A. Hinz, J. M. Goicoechea, *Angew. Chem. Int. Ed.* **2016**, 55, 15515-15519.
- [15] C. Camp, N. Settineri, J. Lefèvre, A. R. Jupp, J. M. Goicoechea, L. Maron, J. Arnold, *Chem. Sci.* **2015**, 6, 6379-6384.
- [16] A. R. Jupp, M. B. Geeson, J. E. McGrady, J. M. Goicoechea, *Eur. J. Inorg. Chem.* **2016**, 2016, 639-648.
- [17] S. Alidori, D. Heift, G. Santiso-Quinones, Z. Benk, *Chem.-Eur. J* **2012**, 18, 14805.
- [18] Y. Wu, L. Liu, J. Su, J. Zhu, Z. Ji, Y. Zhao, *Organometallics* **2016**, 35, 1593-1596.
- [19] G. Becker, K. Hübner, *Z. Anorg. Allg. Chem.* **1994**, 620, 405-417.
- [20] S. Alidori, D. Heift, G. Santiso-Quinones, Z. Benkő, H. Grützmacher, M. Caporali, L. Gonsalvi, A. Rossin, M. Peruzzini, *Chem.* **2012**, 18, 14805-14811.
- [21] S. E. Bradforth, E. H. Kim, D. W. Arnold, D. M. Neumark, *J. Chem. Phys.* **1993**, 98, 800-810.
- [22] T. H. Dunning Jr., K. A. Peterson, A. K. Wilson, *J. Chem. Phys.* **2001**, 114, 9244-9253.
- [23] T. Zeng, D. G. Fedorov, M. Klobukowski, *J. Chem. Phys.* **2011**, 134, 024108.

Heavyweight anions. Four heavier homologues of cyanate and thiocyanate ECX^- ($E = N, P, As$; $X = O, S, Se$) anions have been investigated via a joint approach employing negative ion photoelectron spectroscopy, photoelectron imaging spectroscopy, and quantum chemical computations. The obtained electronic structures, electron affinities (EAs), and spin-orbit (SO) splittings serve as critical points to complete EA and SO matrixes for the $PnCCl^*$ family from the 1st to the 3rd row of both pnictogen and chalcogen series.



Qinqin Yuan,^[a] Frank Tambornino,^[b,c] Alexander Hinz,^[d] Weston Thatcher Borden,^[e] Jose M. Goicoechea,^[b] Bo Chen,^[f] Xue-Bin Wang ^[a]

Page No. – Page No.

Photoelectron spectroscopy and theoretical studies of $PCSe^-$, $AsCS^-$, $AsCSe^-$, and $NCSe^-$: Insights into the electronic structures of the whole family of ECX^- ($E = N, P$, and As ; $X = O, S$, and Se) anions